Monitoring the Catastrophic Flood With GRACE-FO and Near-Real-Time Precipitation Data in Northern Henan Province of China in July 2021

Cuiyu Xiao, Yulong Zhong, Wei Feng, Wei Gao, Zhonghua Wang, Min Zhong, and Bing Ji

***Abstract*—Zhengzhou and its surrounding areas, located in northern Henan Province, China, receive continuous extreme rainfall from July 17 to July 22, 2021. Northern Henan Province experiences extensive flash floods and urban floods, causing severe casualties and property damage. Understanding the variation of hydrologic features during this flood event could be valuable for future flood emergency response work and flood risk management. This study first demonstrates the rainstorm process based on near-real-time precipitation data from the China Meteorological Administration Land Data Assimilation System (CLDAS-V2.0). To meet the temporal resolution required for monitoring this short-term flood event, reconstructed daily terrestrial water storage anomalies (TWSAs) based on GRACE and GRACE-FO data and CLDAS-V2.0 datasets are first introduced. The spatial and temporal evolution of the reconstructed daily TWSA is analyzed in the study area during this heavy rainfall event. We further employ a wetness index based on the reconstructed daily TWSA for flood warnings. Furthermore, the modeled soil moisture data and daily runoff data are used for flood monitoring. Results show that the reconstructed daily TWSA increases by 437.7 mm in just six days (from July 17 to July 22, 2021), with a terrestrial water storage increment of 9.4 km^3. Compared with ITSG-Grace2018, the reconstructed daily TWSA has better potential for near-real-time flood monitoring for short-term events in a small region. The wetness index derived from reconstructed daily TWSA is potential for flood early warning.**

***Index Terms*—Flood, GRACE-FO, northern Henan Province, precipitation reconstruction, rainstorm.**

Manuscript received 28 February 2022; revised 5 September 2022 and 24 October 2022; accepted 17 November 2022. Date of publication 21 November 2022; date of current version 7 December 2022. This work was supported in part by the National Natural Science Foundation of China under Grants 42004073, 41874091, 41874095, and 42074074, in part by the Fundamental Research Funds for the Central Universities, China University of Geosciences (Wuhan) under Grant 26420190050-CUGL190805, in part by the Open Fund of State Key Laboratory of Remote Sensing Science under Grant OFSLRSS202107, in part by the Natural Science Fund for Distinguished Young Scholars of Hubei Province, China under Grant 2019CFA091, and in part by The Second Tibetan Plateau Scientific Expedition and Research Program (STEP) under Grant 2019QZKK0206. *(Corresponding author: Yulong Zhong.)*

Cuiyu Xiao and Wei Gao are with the School of Geography and Information Engineering, China University of Geosciences, Wuhan 430078, China (e-mail: cyxiao@cug.edu.cn; cuggaowei@hotmail.com).

Yulong Zhong is with the School of Geography and Information Engineering, China University of Geosciences, Wuhan 430078, China, and also with the Artificial Intelligence School, Wuchang University of Technology, Wuhan 430223, China (e-mail: zhongyl@cug.edu.cn).

Wei Feng and Min Zhong are with the School of Geospatial Engineering and Science, Sun Yat-sen University, Zhuhai 519085, China (e-mail: fengwei@mail.sysu.edu.cn; zhongm63@mail.sysu.edu.cn).

Zhonghua Wang is with the Wuhan Geotechnical Engineering and Surveying Co., Ltd., Wuhan 430022, China (e-mail: wangzhonghua@whu.edu.cn).

Bing Ji is with the Department of Navigation Engineering, Naval University of Engineering, Wuhan 430033, China (e-mail: jibing1978@126.com).

Digital Object Identifier 10.1109/JSTARS.2022.3223790

I. Introduction

DUE to the combined influence of the Yellow-Huai low vortex, the western Pacific subtropical high pressure, and the continental high pressure [1], a continuous heavy rainfall event occurs in Henan Province, China, from July 17 to July 23, 2021. Many areas in Henan Province suffer from rainstorms, large rainstorms, and even extraordinary rainstorms. The duration of this rainfall is long, the amount of rainfall is copious, and the period and area where the heavy rainfall occurs are relatively concentrated. According to the Monthly Water Report from the Department of Hydrology and Water Resources of Henan, many small and medium-sized rivers in Henan Province exceed their warning water levels, regional mega-floods occur in the upstream of Weihe River and Jialu River, and 14 large and medium-sized reservoirs exceed their historical highest water levels since their construction. The northern and western areas of Henan Province suffer from flash floods and extensive urban floods. This flood event causes severe damage to people's lives and property safety. In recent decades, flood events have occurred increasingly frequently [2], [3], [4], so monitoring the process of the flood is expected to be essential.

The initial state of terrestrial water storage (TWS) is a significant factor that is closely linked to the generation and magnitude of a flood [5], [6]. TWS is the integration of soil moisture (SM), snow, surface water, and groundwater [7], [8]. Terrestrial water storage change (TWSC) reflects the state of accumulated precipitation, evapotranspiration, and surface and (subsurface) runoff [9], [10], [11]. However, it is challenging to monitor TWS with traditional methods [12]. Terrestrial water storage anomalies (TWSAs) derived from the Gravity Recovery and Climate Experiment (GRACE) satellite gravity mission [13] provide a unique means to monitor extreme hydrological events. Chen et al. [9] assessed the 2009 exceptional Amazon flood and interannual TWSC observed by GRACE and further confirmed the unique role of GRACE in describing large-scale extreme climate events. Tangdamrongsub et al. [14] studied the TWS variations and identified flood events over the Tonlé Sap basin in Cambodia between 2002 and 2014 using GRACE and MODIS satellite data, demonstrating that GRACE data is an effective tool for flood monitoring.

GRACE data can be used not only for flood monitoring but also for flood potential assessment. Reager and Famiglietti [5] established a flood potential index (FPI) by applying monthly GRACE-derived TWSA and precipitation observations from the Global Precipitation Climatology Project at the regional scale. FPI reflects effective storage capacity at a certain catchment and estimates a range of allowable precipitation. Molodtsova et al. [15] validated the efficiency of the GRACE-based FPI for evaluating flood potential in the United States and found a good agreement between the FPI and the observed floods. Many scholars have widely applied this FPI to assess the flood potential of many river basins around the world. Its performance of indicating large-scale floods was confirmed, such as in the Niger Basin [16], the Pearl River Basin [17], and the Yangtze River Basin [18], [19], [20]. Sun et al. [21] analyzed the hydrological state in Yangtze River Basin and found that FPI, calculated from the GRACE-derived TWSA and Tropical Rainfall Measuring Mission data, can identify flood events in the Yangtze River Basin. However, they emphasized that for smaller region or short-term flood events, FPI may not be reliable.

The GRACE-derived flood studies mentioned earlier are based on the monthly GRACE products. But flooding as a short-term hydrological event may be triggered only by a short heavy rainstorm [22], [23]. Thus, flood monitoring needs data with comprehensive areal coverage, low latency, and high spatiotemporal resolution [24]. Kurtenbach et al. [25] first tried to obtain the daily solutions based on GRACE L1B data using a Kalman filter approach. For the first time, Gouweleeuw et al. [26] evaluated major flood events in the Ganges–Brahmaputra Delta in 2004 and 2007 using daily GRACE gravity field solutions based on a Kalman filter approach. They assessed ITSG-Grace2014 daily solutions and the GFZ RBF solutions against daily river runoff data and found that the two daily GRACE gravity field solutions show good agreement with river flow, confirming the potential of the two daily solutions for large-scale flood monitoring. However, the current publicly released daily gravity field solutions such as ITSG-Grace2018 [27], with latency in data product processing and release of about several months, cannot meet the near real-time monitoring for flood events. Humphrey and Gudmundsson [28] used a statistical model trained with GRACE data to reconstruct climate-driven monthly and daily TWSA at a spatial resolution of 0.5° based on GRACE products and meteorological forcing datasets. Based on the statistical model used in Humphrey and Gudmundsson [28], we introduce the reconstructed daily TWS anomalies to study this short-duration flood in Henan Province. The latency in obtaining daily TWSAs is shorter than daily ITSG-Grace2018 gravity field solutions. Moreover, since the ITSG-Grace2018 Kalman smoothed daily solutions are constrained within the least square adjustment [29], the actual spatial resolution of the daily solutions is lower than the monthly solutions (∼300 km). The reconstructed daily TWSAs based on near-real-time precipitation data maybe have a higher spatial resolution.

Wetness conditions significantly influence the flood generation of a catchment [30]. European Gravity Service for Improved Emergency Management defined a wetness index (WI) as an effective indicator for early hydrological extremes warning [31]. The WI, which is established on daily gravity data, as a data layer, has been incorporated into the European Commission's Copernicus Global Flood Awareness System (GloFAS) platform. In this study, the WI calculated from the reconstructed daily TWSA is used to evaluate the predisposition of a catchment to flooding.

Therefore, the main objectives of this study are: presenting the catastrophic flood based on reconstructed daily TWSA and precipitation, and exploring the reliability of WI derived from reconstructed daily TWSA. This study begins with a description of the study area in Section II. Section III introduces the data and methods used in this study. In Section IV, the situation of the "July 20 heavy rainstorm in northern Henan Province" is presented. In addition, we demonstrate the temporal and spatial change of daily TWSA, compare the daily river discharge with WI, and analyze the SM state in the study area during this heavy rainstorm event. Section V is the discussion of this study. Finally, we draw our conclusions in Section VI.

II. Study Area

The flooding area boundary is generated based on the accumulated precipitation from July 16 to July 23, 2021, with the contour method adopted in this study. The study area is in northern Henan Province, with a longitude range of 112–115 °E and a latitude range of 34–37 °N. It includes the regions with severe precipitation in Zhengzhou, Jiaozuo, Xinxiang, Hebi, and Anyang cities and its total area is ∼21582 km^2. The topography of the study area is high in the western part where Taihang mountain is located and low in the eastern region.

It has a temperate monsoon climate with four distinct seasons and frequency meteorological and flood disasters [32], [33], [34], [35]. Winter is cold, while summer is hot with plenty of sunlight and precipitation. The seasonal distribution of rainfall is uneven and mainly concentrates in summer. The area spans three major basins, the Yellow River Basin, the Hai River Basin, and the Huai River Basin. There are many small and medium-sized rivers, including the Wei River, the Communist Canal, and the Qi River with hydrometric stations such as Hehe Station, Jixian Station, Liuzhuang Station, Gaocheng Station, and Xinzheng Station.

III. Data and Methods

A. Data

1) GRACE Data: Monthly TWSA is from the CSR RL06 GRACE/GRACE-FO mascon solutions (CSRM) released by the Center for Space Research (CSR) at The University of Texas at Austin. CSRM is calculated with regularization constraints and processed without extra smoothing spatial or empirical de-striping or filtering [36]. The original spatial resolution of CSR Mascon is 1° × 1° [37], and represented to 0.25° × 0.25° for further application. This study utilizes the CSRM to perform the time-series analysis of monthly TWSA and demonstrate the spatial distribution of monthly TWSA in northern Henan Province. Besides, the long-term CSRM from GRACE and GRACE-FO are also used to calibrate and reconstruct the daily TWSAs.

The ITSG-Grace2018 daily solutions are also used in this study for comparison. It is a GRACE-only gravity field solution based on GRACE L1B RL03 data and the atmosphere and ocean dealiasing product [27], [38]. The constrained daily solutions, which are Kalman smoothed [29], have the full signal as the official GRACE monthly products. The spatial resolution of the constrained daily solutions is 1° × 1°. We compare the ITSG-Grace2018 daily TWSA with reconstructed daily TWSA to assess their performance in the study area.

2) CLDAS-V2.0 Data: It is the unexpected heavy rainfall that leads to this severe flood event in Henan Province. Therefore, precipitation data are significant for analyzing this flood event. We use CLDAS-V2.0 near-real-time precipitation data to study this rare rainfall event [39]. The source data of precipitation include observations from more than 2400 national automatic stations and ∼40000 regional automatic weather stations in China [40]. Therefore, this product has better quality compared with its international counterparts in the China region. It has a higher spatial and temporal resolution with latency in data processing and releases only about 2 days. In addition, CLDAS-V2.0 2m temperature data is used to reconstruct daily TWSA. The daily precipitation and 2m temperature from CLDAS-V2.0 from January 2020 to December 2021 are used. SM has an important influence on the generation of rapid runoff and flash floods [41]. We use CLDAS SM products to analyze the SM condition of the study area. CLDAS-2.0 SM product has five vertical layers (0–5, 0–10, 10–40, 40–100, and 100–200 cm) [42], [43]. We convert the data of each of the four vertical layers (0–10, 10–40, 40–100, and 100–200 cm) into the form of equivalent water thickness and then added them together.

3) CGDPA Data: China Gauge-based Daily Precipitation Analysis (CGDPA) is a gridded daily precipitation analysis over Mainland China, developed based on the optimal interpolation method [44]. It has a high spatial resolution of 0.25° × 0.25° with about 2400 station observations in China [45], [46]. The daily precipitation from CGDPA from January 2000 to December 2019 is collected for this study, considering the storage time to equilibrium at the start of the reconstruction as mentioned by Humphrey and Gudmundsson [28], Humphrey et al. [47]. It is one of the fundamental data for the reconstruction of daily TWSA.

4) GLDAS Data: Global Land Data Assimilation System Version 2 (GLDAS-2.2) Catchment Land Surface Model (CLSM) is also used to analyze the daily SM condition. GLDAS-2.2 CLSM daily data is the new product in the Goddard Earth Sciences Data and Information Services Center archive with a spatial resolution of 0.25° × 0.25°. The total terrestrial water anomaly observation from the GRACE mission was assimilated into Catchment Land Surface Model [48]. The model simulations are forced with the meteorological analysis fields from the operational European Centre for Medium-Range Weather Forecasts (ECMWF) Integrated Forecasting System. But the meteorological forcing fields are excluded in the GLDAS-2.2 daily product because of the data agreement with ECMWF. Moreover, the GLDAS-2.2 CLSM product divides the soil layer into three layers, and we sum them up in the same way as the CLDAS-2.0 product.

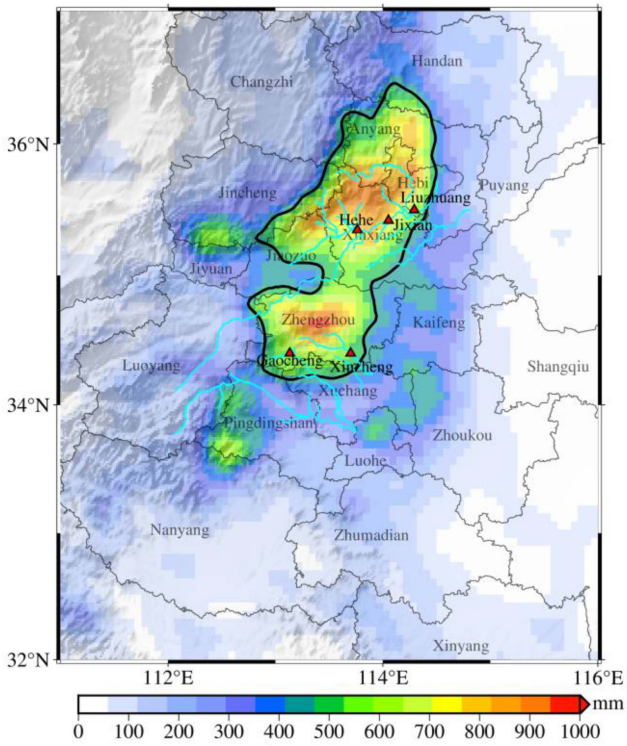

Fig. 1. Map of the study area. The thick black line is the study area boundary defined in this study. The bottom map shows the topographic relief with the spatial distribution of accumulated rainfall from 16 to 23 July superimposed on the top layer. The blue line curves the major rivers in this region, and the red triangles represent the location of hydrometric stations.

5) Runoff Data: Daily runoff data of the five typical hydrometric stations is collected from the Information Center, Ministry of Water Resources, China. The locations of these five hydrometric stations are shown in Fig. 1.

6) Temperature Data: We use the daily temperature data from the CN05.1 dataset to reconstruct daily TWSA. The CN05.1 dataset, constructed by the "anomaly approach" during the interpolation, is a gridded daily observation dataset based on over 2400 gauge stations in China [49]. The spatial coverage is 69.75 °E–140.25 °E, 14.75 °N–55.25 °N. It includes four variables: daily mean, minimum and maximum temperature, and daily precipitation. This dataset can be used to detect and monitor climate change and has potential applications in agriculture, hydrology [50], and ecology.

Table I is an overview of all the datasets mentioned earlier.

B. Methods

1) GARCE-TWSA Reconstruction: Humphrey and Gudmundsson [28] proposed a linear statistical model from basic principles of hydrological modeling to describe approximately the temporal evolution of the storage. The model can be formulated as follows:

$$TWS(t) = (TWS(t-1))e^{-1/\tau(t)} + P(t) \tag{1}$$

where *t*, *TWS(t)*, and *P(t)* represent the daily time vector, the storage, and the precipitation input in the *t*th day, respectively.

TABLE I
SUMMARY OF THE DATASETS USED IN THIS STUDY

Dataset	Time span	Spatial resolution	Temporal resolution	Data source
CSRM RL06	2002–2021	0.25°	Monthly	http://www2.csr.utexas.edu/grace/RL06_mascons.html
ITSG-Grace2018	2021.1–2021.7	1°	Daily	http://icgem.gfz-potsdam.de/series/03_GRACE_other/ITSG/ITSG-Grace2018/daily
CLDAS-V2.0	2017–2021	0.0625°	Daily	https://data.cma.cn/
CGDPA	2000–2019	0.5°	Daily	https://data.cma.cn/
GLDAS-2.2 CLSM	2017–2021	0.25°	Daily	https://daac.gsfc.nasa.gov/datasets/GLDAS_CLSM025_DA1_D_2.2/summary?keywords=GLDAS
CN05.1	2000–2019	0.25°	Daily	Contact with the authors
Runoff	2021		Daily	http://xxfb.mwr.cn/sq_dxsk.html

Reference: CSRM RL06 [55], ITSG-Grace2018 [27], CLDAS-V2.0 [39], CGDPA [44], GLDAS-2.2 CLSM [48], and CN05.1 [49].

And $\tau(t)$ is the residence time of the water store. Small (large) values of the residence time indicate that the input water leaves the catchment quickly (slowly) owing to runoff or evapotranspiration. It is temperature-dependent, which can be expressed by the following equation:

$$\tau(t) = a + b \cdot Tz(t) \tag{2}$$

where a and b are the positive-calibrated model parameters, and $T_Z(t)$ is the transformed original de-trended daily air temperature.

The modeled daily TWS is further averaged to GRACE "month," then the reconstructed parameters are calibrated between deseasonalized and detrended GRACE TWS and modeled TWS, such that

$$TWS_{GRACE} = \beta \cdot TWS_{REC} + \varepsilon \tag{3}$$

where β is the calibrated parameter, and ε represents the error term. The TWS_{GRACE} and TWS_{REC} are detrended and deseasonalized. In this study, the calibrated period is January 2003 to December 2020. The daily TWSA can be reconstructed with near-real-time precipitation and temperature data when calibrated parameters are obtained.

More details about the reconstructed method are recommended to refer to Humphrey and Gudmundsson [28]. The resolution of reconstructed daily TWSAs in this study is presented as 0.5° × 0.5°, considering the different resolutions of input data.

2) Wetness Index: The WI [31] is calculated based on the reconstructed daily TWSA ($TWSA_{tot}$), expressing in equivalent water thickness. $TWSA_{tot}$ can be decomposed into the trend term ($TWSA_{trend}$), the mean seasonal cycle ($TWSA_{seas}$) and the interannual and subseasonal variation ($TWSA_{interannual+subseas}$)

$$TWSA_{tot} = TWSA_{trend} + TWSA_{seas} + TWSA_{interannual+subseas}. \tag{4}$$

WI represents the departure of $TWSA_{tot}$ from the $TWSA_{seas}$ after removing $TWSA_{trend}$, expressing in dimensionless unit

$$WI = \frac{D}{S} = \frac{TWSA_{interannual+subseas}}{S}. \tag{5}$$

D equals interannual variation plus subseasonal terms, and S is standard deviation, a measure of the variation of D.

In fact, we can obtain the $TWSA_{interannual+subseas}$ term from the reconstruction model directly in this study.

IV. RESULTS

A. Rainstorm Situation

To understand the process of rainfall, the CLDAS-V2.0 near-real-time precipitation data is used to draw the daily rainfall distribution map. As shown in Fig. 2, heavy rain (25–50 mm) and rainstorms (50–100 mm) occur in the study area, with some regions experiencing large rainstorms (100–250 mm) on July 18. On July 19, most areas in Henan Province receive daily precipitation of over 25 mm, and western Zhengzhou City and southwestern Pingdingshan City suffer extraordinary rainstorms (250–400 mm), with an average rainfall of 95.7 mm in the study area. The daily average rainfall on July 19 is as high as 199 mm (4.3 km^3, about the water volume of 307 the West Lake, a famous lake in China) in the study area. On July 20, the rainstorm intensity increases, with the area whose daily precipitation is over 100 mm exceeding 45000 km^2. The rainstorm center is in the western part of Zhengzhou City on that day, reaching the level of an extraordinary rainstorm. On the next day, the rainstorm center moves northward. The daily rainfall in some areas of Xinxiang City, Hebi City, and Anyang City even exceeds 400 mm, with a mean daily rainfall of 174.5 mm in the study area. On July 22, the rainfall extent and amount in Henan Province decrease remarkably, indicating that this continuous rainstorm event reached its end, with a mean daily rainfall of 31.9 mm in the study area.

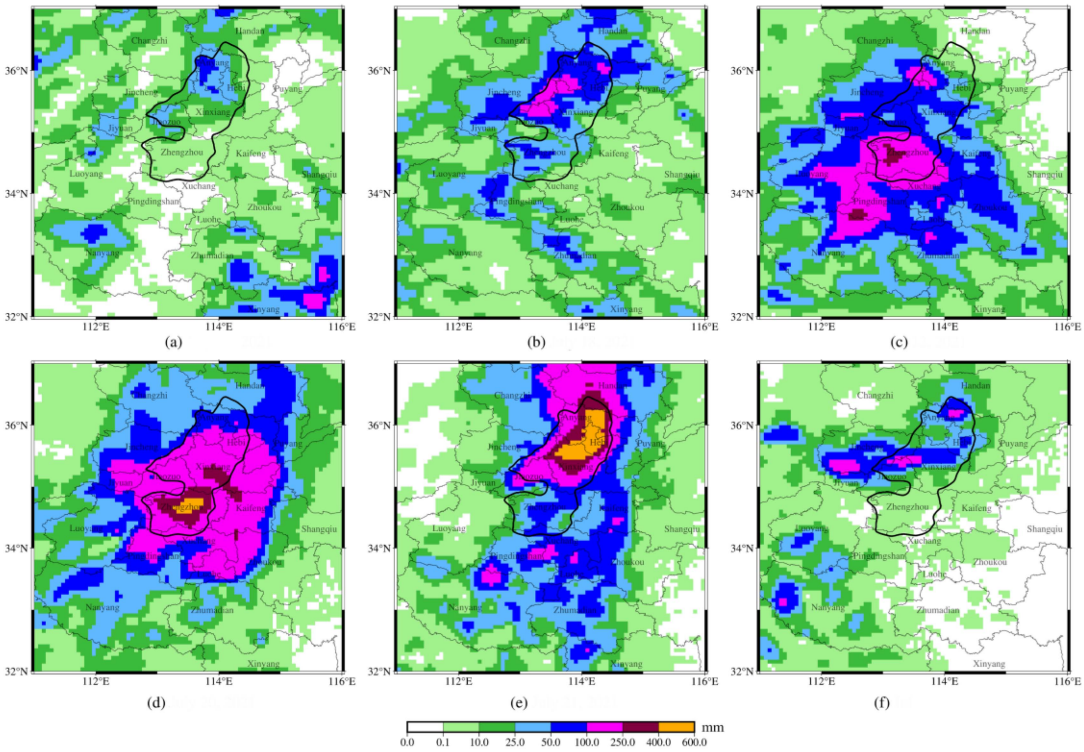

Fig. 2. Daily rainfall distribution map in Henan province from July 17 to July 22, 2021. (a) July 17, 2021. (b) July 18, 2021. (c) July 19, 2021. (d) July 20, 2021. (e) July 21, 2021. (f) July 22, 2021.

B. Temporal and Spatial Variations of TWSA

Fig. 3 shows the spatial distribution of reconstructed daily TWSA and ITSG-Grace2018 daily TWSA during the storm. Reconstructed daily TWSA exhibits similar spatial distribution to that of precipitation. The daily TWSAs of grid cells in the study area relative to the mean value between 2004 and 2009 are at a low positive or even negative value on July 16 (not shown), while the variability of TWSA increases significantly from the south to the north of the study area as the rainstorm center moved north. TWSA in several grids exceeds 300 mm (Fig. 3). Fig. 3(e) and (f) show the spatial distribution of TWSA on July 26 and July 31. It can be seen that TWSA in most grids of the study area remains a high positive value after the rainstorm. Compared with the reconstructed daily TWSA, ITSG-Grace2018 daily solutions do not characterize the spatial variability of TWSA well during this rainstorm event.

The reconstructed daily TWSA rises by 437.7 mm with a water storage gain of 9.4 km^3 from July 17 to July 22. It reaches its maximum value of 475.6 mm on July 22 (Fig. 4), which is also the maximum value in the study area since April 2002. However, ITSG-Grace2018 daily TWSA shows a smaller variation and cannot reflect the actual TWS changes well during this heavy rainfall event. The time series of reconstructed daily TWSA and SM of two products from June to August of the last five years are also analyzed (Fig. 5). Obviously, both the daily TWSA and SM after 16 July 2021 are significantly higher than those in previous years, reflecting the large magnitude of the impact caused by this rainstorm.

After the heavy rainstorm, the value of TWSA is much higher than that of SMSA (Fig. 4). To trace this different performance, the other two components in TWS are analyzed. The in-situ groundwater table data from the monthly groundwater status report (MGSR) published by Hydrological and Water Resources Monitoring and Forecasting Centre, Ministry of Water Resources, China (MGSR-MWR), is further collected (Fig. 6). Since the groundwater table data published by MGSR-MWR is only a monthly mean value, they do not show a clear increase in groundwater level from June to July. However, the monthly average groundwater level increases in August compared with July. It indicates the process of groundwater recharge from SM. Moreover, urban flooding in the study area is severe during flood period, which leads to significant increase in surface water that is not included in SMSA. And there are uncertainties in the reconstructed TWSA and SM data. These factors may partly explain the difference between TWSA and SMSA after this flood (Fig. 4).

The spatial distribution of monthly TWSA of CSRM from June to August for 2020 and 2021 is presented in Fig. 7. It is shown that the TWSA in and around the study area is surplus in July and August 2021. The average rainfall of Henan Province in July 2021 is 90% more than the average value of the same period in past years. The monthly TWSA from CSRM in the study area reaches 127.5 mm in July 2021, which is 136.2 mm higher than the same month last year. In addition, the TWSA from CSRM in July 2021 is 151.8 mm higher than in June 2021, while the TWSA in July 2020 is 91.5 mm higher than in June 2020. The TWSA continues to rise in August and stays in high

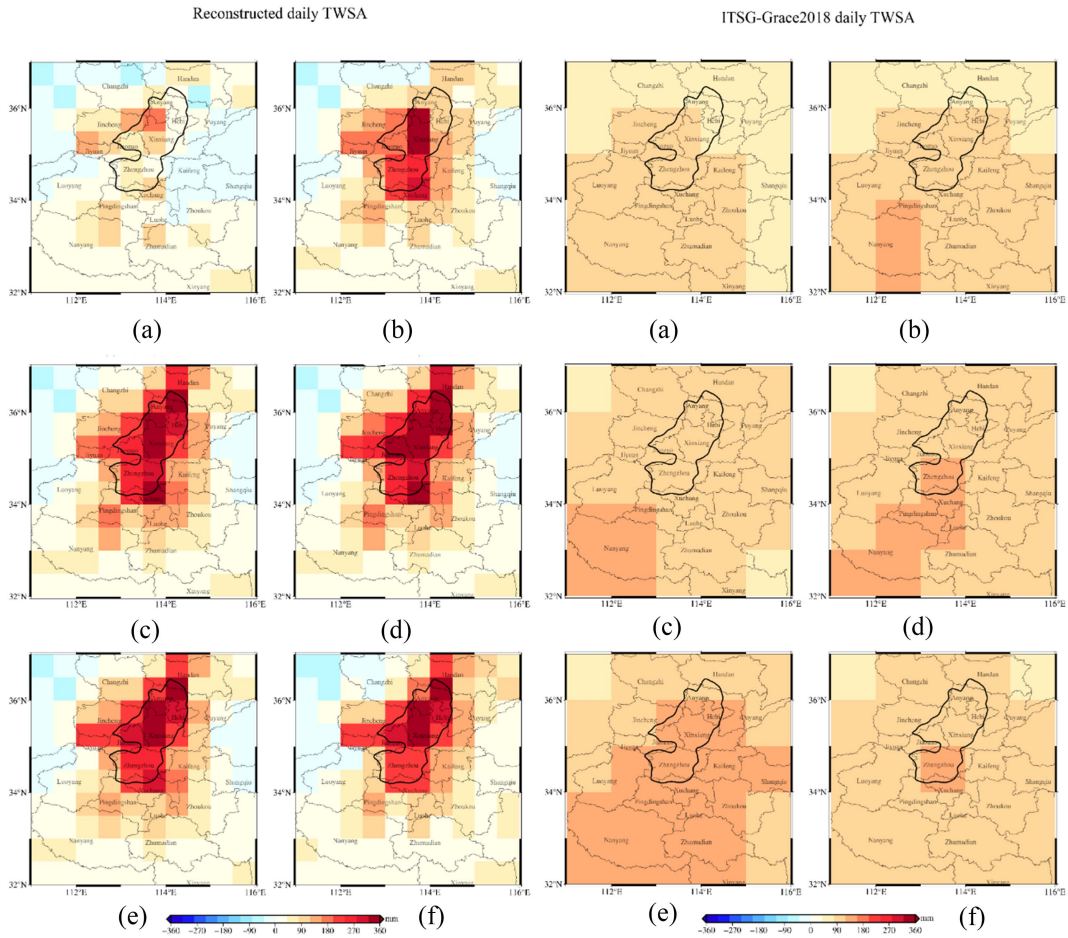

Fig. 3. Spatial distribution of reconstructed daily TWSA (0.5° × 0.5°). (a) July 19, 2021. (b) July 20, 2021. (c) July 21, 2021. (d) July 22, 2021. (e) July 26, 2021. (f) July 31, 2021. And ITSG-Grace2018 daily TWSA (1° × 1°) in July with the seasonal cycle and the linear trend removed. (a) July 19, 2021. (b) July 20, 2021. (c) July 21, 2021. (d) July 22, 2021. (e) July 26, 2021. (f) July 31, 2021.

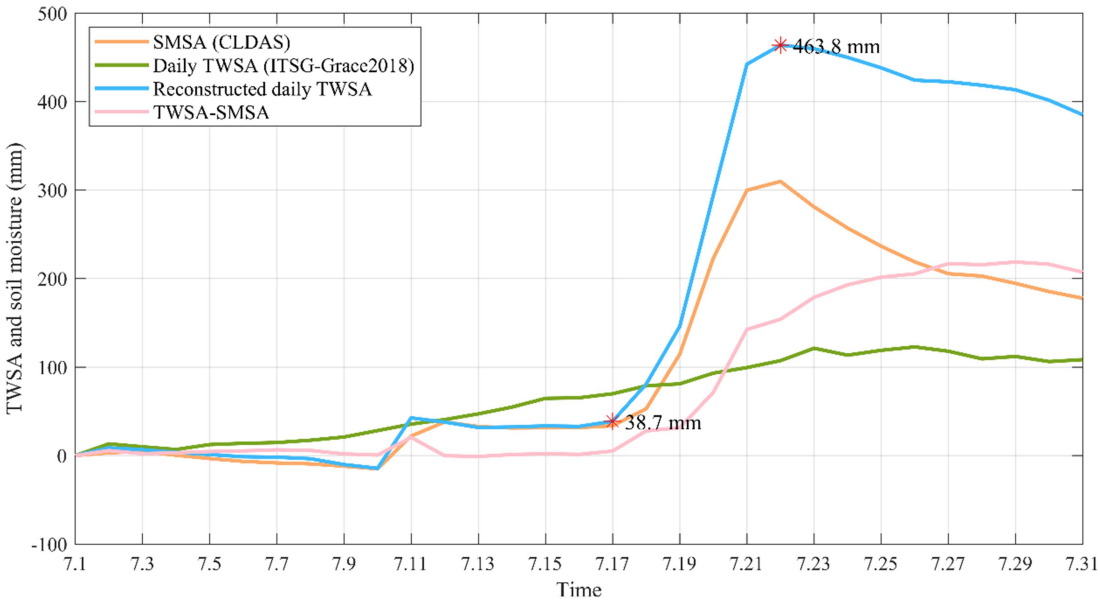

Fig. 4. Comparison of time series of de-trended and deseasonalized reconstructed daily TWSA, ITSG-Grace2018 daily TWSA, SM derived from CLDAS-V2.0 data and difference between TWSA and SMSA in the study area in July 2021. The starting points are set to 0 for comparison.

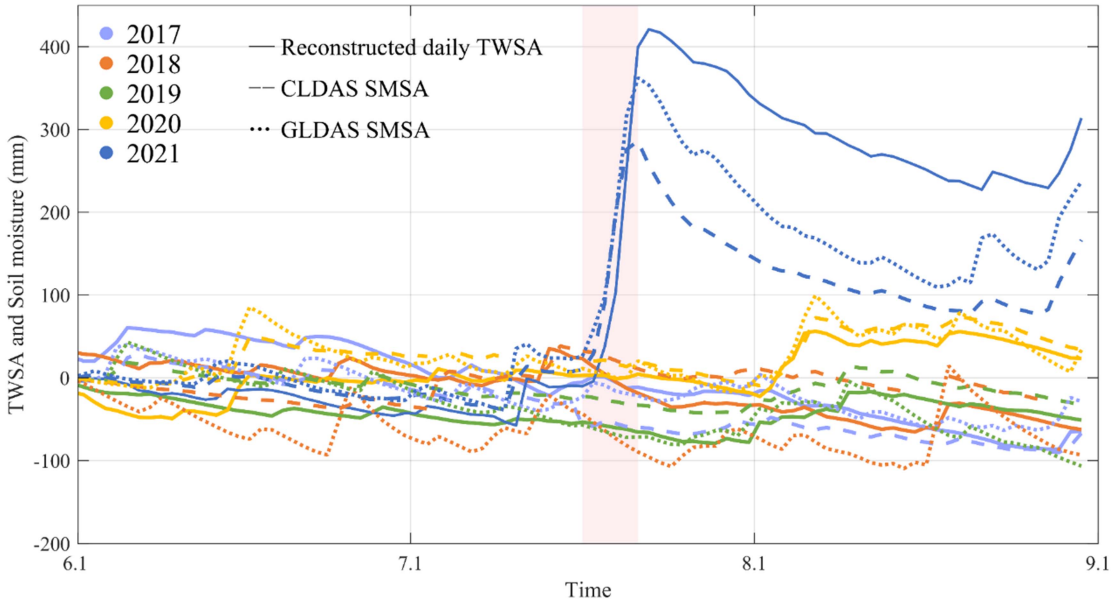

Fig. 5. Time series of reconstructed daily TWSA, SM derived from CLDAS-V2.0 data with part of the data missing and GLDAS V2.2 data from June to August of last five years. The pink shades represent the period from 17 July to 22 July. The starting points are all set to 0 for better viewing.

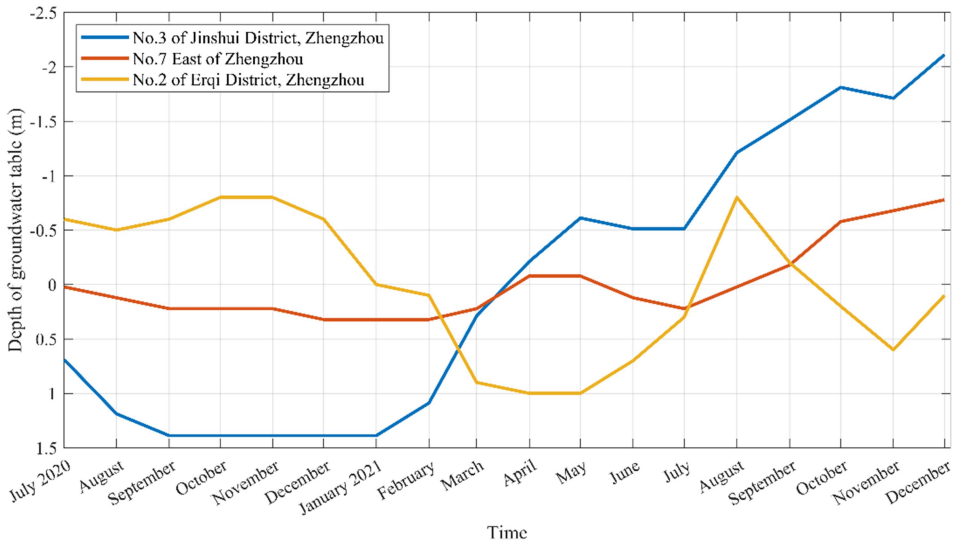

Fig. 6. Depth of groundwater table obtained from three groundwater monitoring wells. It should be noted that No.2 of Erqi District, Zhengzhou is a fissure water well. The mean of January to December 2021 is removed from the depth of groundwater table. Y-axis is reversed for better viewing.

value until December (Fig. 8). We compare the accumulated precipitation from July to December for each year from 2012 to 2021 in Fig. 9(a). The accumulated precipitation from July to December is obviously higher in 2021 than in other years, which has led to the high value of TWSA in the study area [Fig. 9(b)].

The TWSA from JPL Mascon, GSFC Mascon, CSR Level-3, JPL Level-3, GFZ Level-3, and ITSG-Grace2018 daily solutions are also compared in Fig. 8. However, these products cannot capture the increase of TWSA caused by the heavy rainfall in July. Generally, GRACE data is considered suitable only for basins larger than 200000 km^2 [51]. Besides, Kunstmann et al. [52] demonstrated that besides spatial resolution, the signal is also a key factor affecting the application of GRACE to small basins. Fig. 10 presents the ground track of GRACE-FO satellites during July 2021. We find the satellites pass over the study area just 5 times within a month. The period is so short that rapid earth gravity-field variations cannot be adequately sampled [53]. What is more, the satellites pass over the study area only once after the heavy rainstorm in July. The other four crossings are prior to the occurrence or at the onset of the heavy rainfall. These may explain why the monthly TWSAs from different solutions cannot capture the flood-induced TWSA. Therefore, the reconstructed daily TWSA based on near-real-time precipitation data is introduced to analyze this flood event.

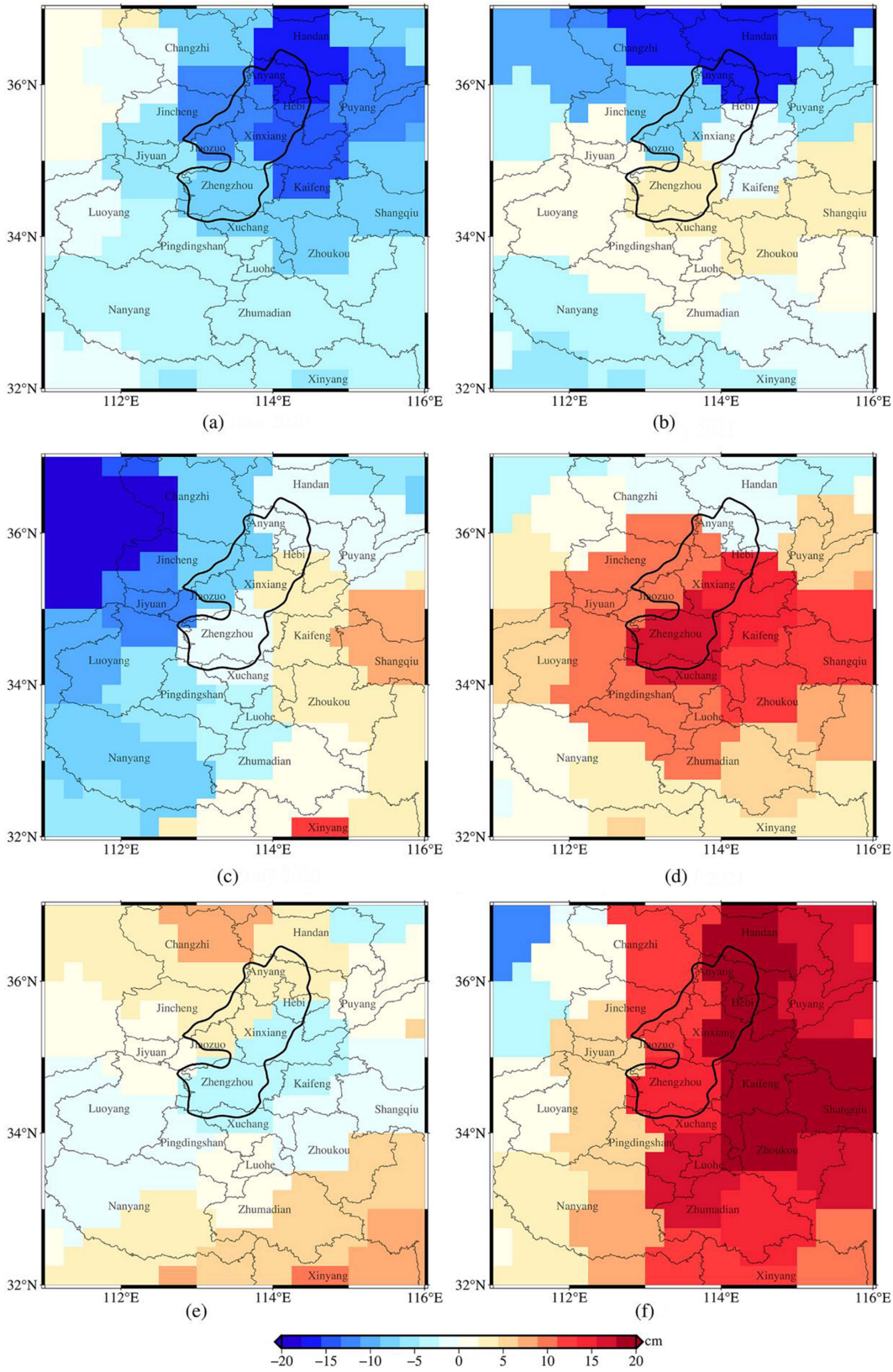

Fig. 7. Spatial distribution of monthly TWSA of CSR Mascon with the seasonal cycle and the linear trend are removed from June to August for 2020 and 2021. (a) June 2020. (b) June 2021. (c) July 2020. (d) July 2021. (e) August 2020. (f) August 2021.

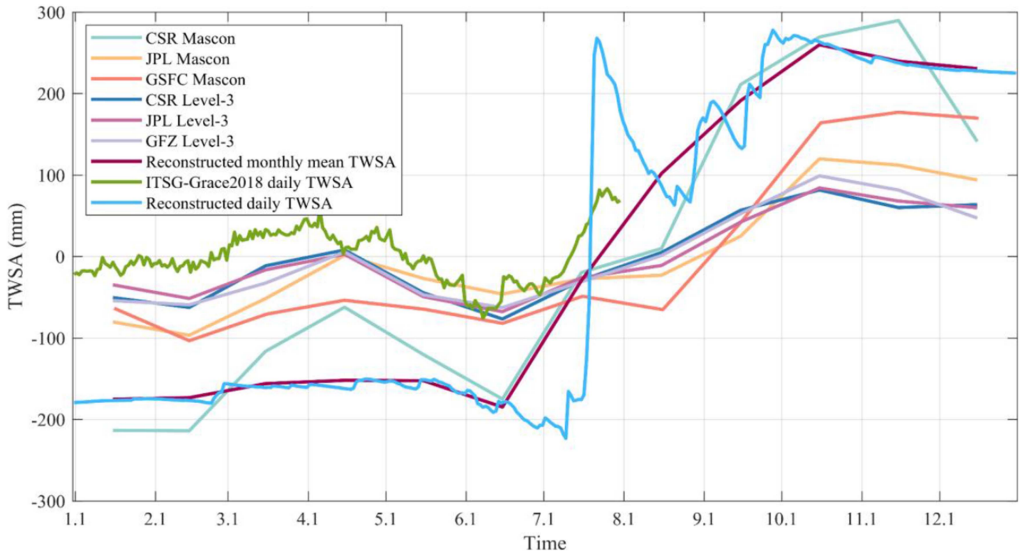

Fig. 8. Time series of monthly/daily TWSA of seven GRACE products and reconstructed monthly/ daily TWSA in the study area during 2021.

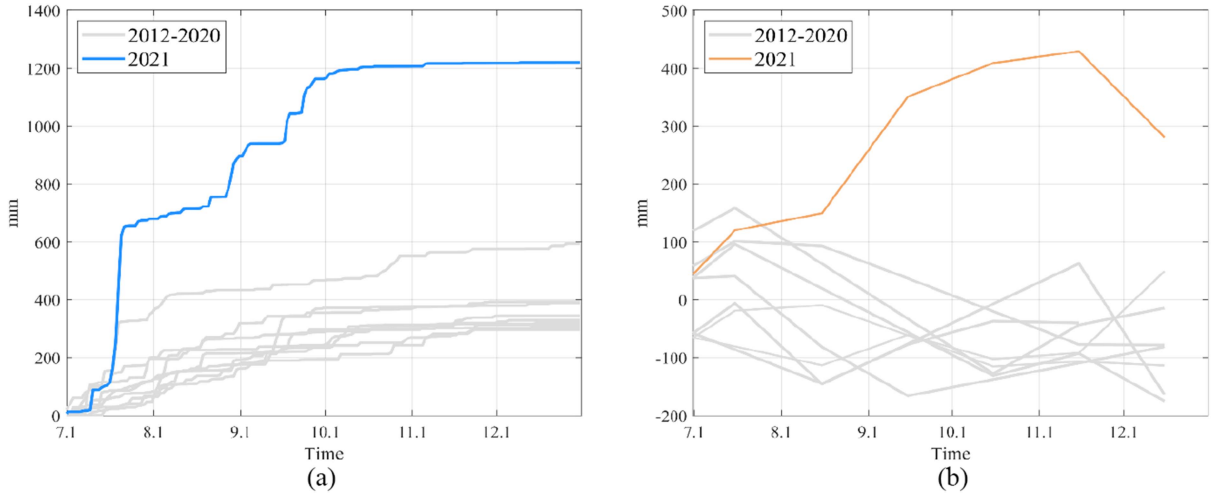

Fig. 9. Accumulated precipitation and TWSA from CSRM with the seasonal cycle and the linear trend removed from July to December for each year from 2012 to 2021. (a) Accumulated precipitation. (b) TWSA.

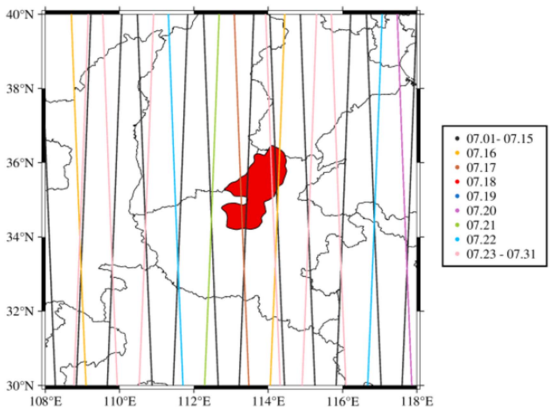

Fig. 10. Ground track of GRACE-FO satellites during July 2021.

V. Discussion

The SM conditions before the rainfall event will influence the flood magnitude and duration [53], [54]. The drier the catchment is, the greater the water storage capacity will be. Thus, the likelihood of flooding will be lower. On the contrary, the wetter the catchment is, the smaller the water storage capacity will become, and the more likely the flood will occur [55]. Therefore, the preceding soil wetness state should not be ignored. We use the SM data from CLDAS-V2.0 to analyze the SM conditions. A smaller rainfall occurs in the study area on July 11 (Fig. 11). Due to this smaller rainfall, the SM increases and reaches 38.0 mm on July 12. It is 20.0th percentile on July 16 (the day before the extreme rainstorm) among the daily SM from April 1, 2017 to July 16, 2021. The preceding rainfall lowers the ability of

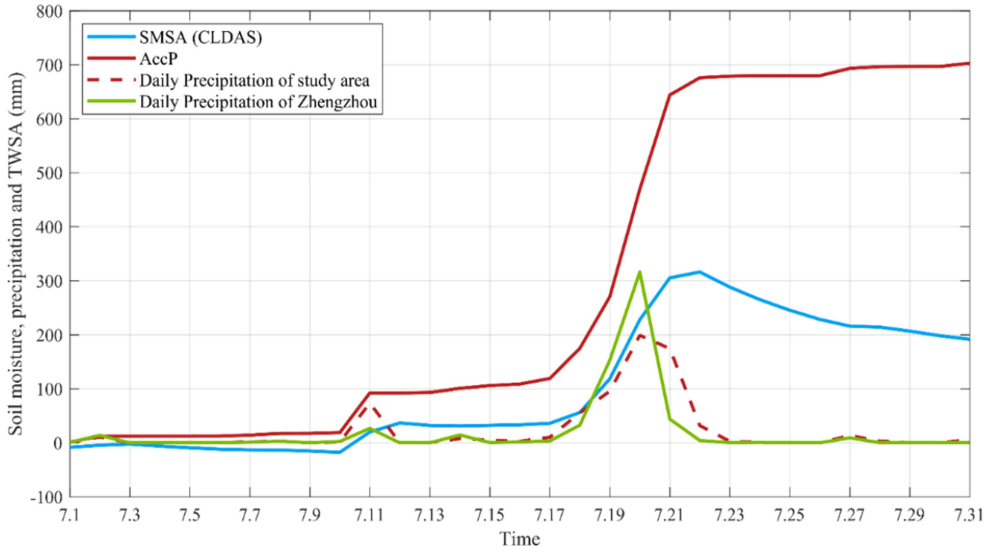

Fig. 11. Time series of SM from CLDAS V2.0, accumulated precipitation (AccP), and daily mean precipitation from CLDAS-V2.0.

the soil layers to store water in the study area and increases the risk of the subsequent flood event. With the occurrence of this violent rainstorm from July 17, SM rises rapidly and reaches the maximum on July 22, which is also the maximum for April 2017 to July 2021. When the soil is already saturated, it cannot store additional water. If it continues to rain, rainfall cannot infiltrate into saturated soil, leading to higher runoff and eventually causing flooding.

Fig. 12 depicts the flood and WI calculated with reconstructed daily TWSA and ITSG-Grace2018 daily TWSA dynamics in detail. The WIs in Xinxiang, Hebi, and Zhengzhou are extracted based on reconstructed daily TWSA from 0.5° lon-lat grid and ITSG-Grace2018 daily TWSA from 1° lon-lat grid, and then we compare them with the daily runoff from the hydrological stations. Due to the limited resolution of these two TWSAs, the extracted time series for different cities may contain some uncertainty. However, as the actual resolution of precipitation data used here is higher than that of GRACE/GRACE-FO data, the actual resolution of reconstructed TWSA may be higher. In fact, the WIs in different cities indeed show some interesting and specific performance.

We assume that the threshold of WI is 2 as Jäggi et al. [31]. If the WI exceeds the threshold, it indicates the catchment closing to storage saturation. At this time, attention should be given to the risk of flooding in the basin. The WI calculated with reconstructed daily TWSA of Xinxiang exceeds the threshold 2 on July 20, while the river discharge measured by Jixian hydrological station and Hehe hydrological station exceeds the dependable flows on July 23 and July 24, respectively [Fig. 12(a)]. This WI based on reconstructed daily TWSA warns of flooding three days in advance. The day WI calculated with reconstructed daily TWSA in Hebi exceeds the assumed threshold is prior to the day the dependable flow is over at the Liuzhuang hydrological station of 2 days. Notably, the river discharge measured by Liuzhuang hydrological station has two peaks and the second peak is greater than the first. It is possibly due to different types of runoffs. Runoff formed by different components produces flow at different rates. But the WIs calculated with ITSG-Grace2018 daily TWSA in Xinxiang, Hebi, and Zhengzhou have never exceeded the assumed threshold in July 2021.

It seems that the warning of WI calculated with reconstructed daily TWSA in Zhengzhou fails to work [Fig. 12(c)]. The WI of Zhengzhou exceeds the assumed threshold on July 20, while the peaks of the two runoffs occur on July 20 and 21, respectively. We consider that this situation may be related to the duration of rainfall excess and the travel time of runoff. Moreover, the overestimate of residence time during the flood period, the catchment area, and the location of the hydrometric stations may be the factors contributing to this situation. Gaocheng hydrometric station is on the upper reaches of the Ying River, while Xinzheng hydrometric station is located at the lower reaches of the Shuangji River (Fig. 1). Therefore, peak values of two flood hydrographs do not appear on the same day. Zhengzhou receives nearly six times as much rainfall on July 19 as on July 18 (Fig. 11). On July 19 the daily precipitation is 166.9 mm and on July 20 it increases to 280.8 mm. The rainfall intensity is so astonishing that the SM increases rapidly. The rate of infiltration decreases as the SM increases. When the precipitation is greater than the soil's infiltration capacity, some of the precipitation cannot afford the time to infiltrate and directly lead to infiltration excess overland flow [54]. As we can see in Fig. 12(c), both flood hydrographs rise and fall rapidly with high peak values. It can be inferred that the duration of rainfall excess and travel is short. These factors limit the potential of WI for flood early warning in Zhengzhou.

In the previous section, we point out the possible reasons why TWSA is higher than SMSA and decrease more slowly than river discharge and SMSA after the rainstorm. As the TWS is the summation of all land water, including surface water, SM, groundwater, etc. The changes in SM and groundwater are more slowly than surface water. Thus, TWS does not decline as quickly as the conventional flood indicators (e.g., stream flow),

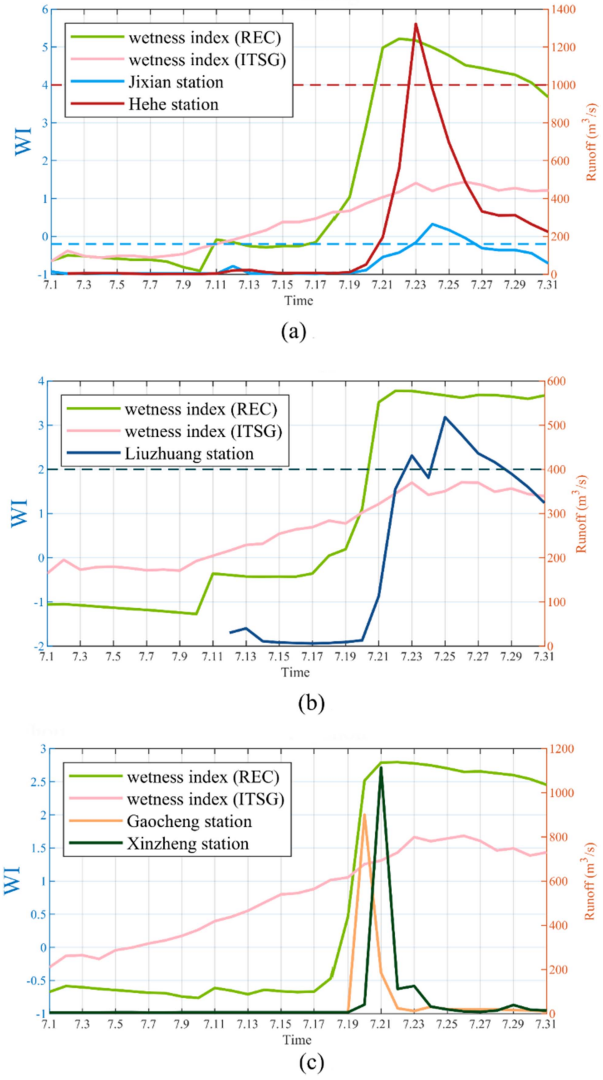

Fig. 12. WI from reconstructed daily TWSA and ITSG-Grace2018 daily TWSA and river discharge measured by hydrometric stations in the study area. The dotted lines represent the dependable flows set by the hydrometric station. (a) Xinxiang. (b) Hebi. (c) Zhengzhou.

and it is difficult to locate the terminate time of flood events based on the TWSA. In addition, the flood warning indexes such as FPI and WI, which are highly correlated with changes in TWS, also cannot reflect the recession of the flood.

Furthermore, the parameters for residence time are calibrated using the long-term precipitation and monthly GRACE TWSA data. This might result in the overestimate of residence time during the catastrophic flood event, during which water tends to leave the region more quickly. These factors limit the potential of reconstructed TWSA for flood monitoring in the study area. In future studies, hydrological variables could be added in (2) in this manuscript, e.g., precipitation or SM, to better characterize the residence time. Moreover, using the flood period as the calibration period may be a good idea when there are enough historical flood events to use for calibrating in the study area.

VI. Conclusion

In this study, we use CLDAS-V2.0 near-real-time precipitation product to analyze the heavy rainstorm process in Henan Province, China in July 2021. The reconstructed daily TWSAs based on CSRM, CLDAS-V2.0 near-real-time precipitation and temperature data, and historical daily precipitation and temperature data are used to study the dynamic changes of TWSA before and after the heavy rainfall in the study area.

The SM data from CLDAS-V2.0 and GLDAS V2.2 datasets are utilized to evaluate the wetness conditions of the study area and the risk of flooding. Additionally, we also compare the GRACE-derived WI with daily river discharge from hydrological stations to assess the potential of the WI in the early flood warnings. We summarize the following conclusions.

1) The reconstructed daily TWSA significantly increases due to the heavy rainfall. It rises by 437.7 mm from July 17 to July 22, 2021, with a water storage increment of 9.4 km^3.
2) Compared with ITSG-Grace2018 daily solutions, the reconstructed daily TWSA better reflects the dramatic increase of daily TWSA caused by the extreme rainfall.
3) The reconstructed daily TWSA shows a good performance in monitoring this short-term flood event and the daily reconstructed-based WI has the potential for early flood warning.

Acknowledgment

The authors would like to thank the Center for Space Research (CSR), University of Texas at Austin and Institute of Geodesy, Graz University of Technology for providing the GRACE data. And also thank the China Meteorological Administration (CMA) for providing the CLDAS-2.0, CGDPA, and CN05.1 data; the Ministry of Water Resources of China for providing the in-situ runoff data and the National Aeronautics and Space Administration for providing the GLDAS-2.2 data. Part of the work in this study forms an advisory report, which is provided to the relevant management department for decision-making.

References

[1] A. Su, X. Lv, L. Cui, Z. Li, L. Xi, and H. Li, "The basic observational analysis of '7.20' extreme rainstorm in Zhengzhou," *Torrential Rain Disasters*, vol. 40, no. 5, pp. 445–454, 2021.
[2] Z. M. Nigatu, D. Fan, W. You, and A. M. Melesse, "Hydroclimatic extremes evaluation using GRACE/GRACE-FO and multidecadal climatic variables over the Nile river basin," *Remote Sens.*, vol. 13, no. 4, 2021, Art. no. 651.
[3] D. Long et al., "Drought and flood monitoring for a large karst plateau in Southwest China using extended GRACE data," *Remote Sens. Environ.*, vol. 155, pp. 145–160, 2014.
[4] C. E. Ndehedehe, "The water resources of tropical West Africa: Problems, progress, and prospects," *Acta Geophysica*, vol. 67, no. 2, pp. 621–649, 2019.
[5] J. T. Reager and J. S. Famiglietti, "Global terrestrial water storage capacity and flood potential using GRACE," *Geophysical Res. Lett.*, vol. 36, no. 23, 2009, Art. no. 2009GL040826.
[6] D. Long et al., "Deriving scaling factors using a global hydrological model to restore GRACE total water storage changes for China's Yangtze river basin," *Remote Sens. Environ.*, vol. 168, pp. 177–193, 2015.

[7] M. Rodell, I. Velicogna, and J. S. Famiglietti, "Satellite-based estimates of groundwater depletion in India," *Nature*, vol. 460, no. 7258, pp. 999–1002, Aug. 2009.

[8] Y. Zhong, W. Feng, V. Humphrey, and M. Zhong, "Human-induced and climate-driven contributions to water storage variations in the Haihe river basin, China," *Remote Sens.*, vol. 11, no. 24, 2019, Art. no. 3050.

[9] J. L. Chen, C. R. Wilson, and B. D. Tapley, "The 2009 exceptional Amazon flood and interannual terrestrial water storage change observed by GRACE," *Water Resour. Res.*, vol. 46, no. 12, 2010, Art. no. 2010WR009383.

[10] D. Long et al., "Global analysis of spatiotemporal variability in merged total water storage changes using multiple GRACE products and global hydrological models," *Remote Sens. Environ.*, vol. 192, pp. 198–216, 2017.

[11] Y. Zhong, M. Zhong, Y. Mao, and B. Ji, "Evaluation of evapotranspiration for exorheic catchments of China during the GRACE era: From a water balance perspective," *Remote Sens.*, vol. 12, no. 3, 2020, Art. no. 511.

[12] W. Yin, L. Hu, S.-C. Han, M. Zhang, and Y. Teng, "Reconstructing terrestrial water storage variations from 1980 to 2015 in the Beishan area of China," *Geofluids*, vol. 2019, 2019, Art. no. 3874742.

[13] B. D. Tapley, S. Bettadpur, M. Watkins, and C. Reigber, "The gravity recovery and climate experiment: Mission overview and early results," *Geophysical Res. Lett.*, vol. 31, no. 9, 2004, Art. no. 2004GL019920.

[14] N. Tangdamrongsub, P. G. Ditmar, S. C. Steele-Dunne, B. C. Gunter, and E. H. Sutanudjaja, "Assessing total water storage and identifying flood events over Tonlé Sap basin in Cambodia using GRACE and MODIS satellite observations combined with hydrological models," *Remote Sens. Environ.*, vol. 181, pp. 162–173, 2016.

[15] T. Molodtsova, S. Molodtsov, A. Kirilenko, X. Zhang, and J. Van-Looy, "Evaluating flood potential with GRACE in the United States," *Natural Hazards Earth Syst. Sci.*, vol. 16, no. 4, pp. 1011–1018, 2016.

[16] D. Idowu and W. Zhou, "Performance evaluation of a potential component of an early flood warning system—A case study of the 2012 flood, lower Niger river basin, Nigeria," *Remote Sens.*, vol. 11, no. 17, 2019, Art. no. 1970.

[17] Z. Huang, J. J. Jiao, X. Luo, Y. Pan, and T. Jin, "Drought and flood characterization and connection to climate variability in the pearl river basin in Southern China using long-term GRACE and reanalysis data," *J. Climate*, vol. 34, no. 6, pp. 2053–2078, 2021.

[18] H. Zhou et al., "Characterizing drought and flood events over the Yangtze river basin using the HUST-grace2016 solution and ancillary data," *Remote Sens.*, vol. 9, no. 11, 2017, Art. no. 1100.

[19] P. Yang et al., "Impacts of climate change-related flood events in the Yangtze river basin based on multi-source data," *Atmospheric Res.*, vol. 263, 2021, Art. no. 105819.

[20] J. Xiong, S. Guo, J. Yin, L. Gu, and F. Xiong, "Using the global hydrodynamic model and GRACE follow-on data to access the 2020 catastrophic flood in Yangtze river basin," *Remote Sens.*, vol. 13, no. 15, 2021, Art. no. 3023.

[21] Z. Sun, X. Zhu, Y. Pan, and J. Zhang, "Assessing terrestrial water storage and flood potential using GRACE data in the Yangtze river basin, China," *Remote Sens.*, vol. 9, no. 10, 2017, Art. no. 1011.

[22] S. Czigány, E. Pirkhoffer, and I. Geresdi, "Impact of extreme rainfall and soil moisture on flash flood generation," *Quart. J. Hung. Meteorological Service*, vol. 114, no. 1/2, pp. 79–100, 2010.

[23] M. Diakakis, "Rainfall thresholds for flood triggering. The case of Marathonas in Greece," *Natural Hazards*, vol. 60, no. 3, pp. 789–800, 2012.

[24] N. Tangdamrongsub, C. Forgotson, C. Gangodagamage, and J. Forgotson, "The analysis of using satellite soil moisture observations for flood detection, evaluating over the Thailand's great flood of 2011," *Natural Hazards*, vol. 108, no. 3, pp. 2879–2904, 2021.

[25] E. Kurtenbach, T. Mayer-Gürr, and A. Eicker, "Deriving daily snapshots of the Earth's gravity field from GRACE L1B data using Kalman filtering," *Geophysical Res. Lett.*, vol. 36, no. 17, 2009, Art. no. 2009GL039564.

[26] B. T. Gouweleeuw et al., "Daily GRACE gravity field solutions track major flood events in the Ganges–Brahmaputra delta," *Hydrol. Earth Syst. Sci.*, vol. 22, no. 5, pp. 2867–2880, 2018.

[27] A. Kvas et al., "ITSG-Grace2018: Overview and evaluation of a new GRACE-only gravity field time series," *J. Geophysical Res., Solid Earth*, vol. 124, no. 8, pp. 9332–9344, 2019.

[28] V. Humphrey and L. Gudmundsson, "GRACE-REC: A reconstruction of climate-driven water storage changes over the last century," *Earth Syst. Sci. Data*, vol. 11, no. 3, pp. 1153–1170, 2019.

[29] E. Kurtenbach et al., "Improved daily GRACE gravity field solutions using a Kalman smoother," *J. Geodynamics*, vol. 59–60, pp. 39–48, 2012.

[30] Y. Tramblay, C. Bouvier, C. Martin, J.-F. Didon-Lescot, D. Todorovik, and J.-M. Domergue, "Assessment of initial soil moisture conditions for event-based rainfall–runoff modelling," *J. Hydrol.*, vol. 387, no. 3/4, pp. 176–187, 2010.

[31] A. Jäggi et al., "European gravity service for improved emergency management (EGSIEM)—From concept to implementation," *Geophysical J. Int.*, vol. 218, no. 3, pp. 1572–1590, 2019.

[32] J.-H. Liang, Y.-H. Jiang, H. Chen, and Y.-C. Wu, "Diagnostic analysis of an exceptionally heavy rain in August 2018," *Guangdong Meteorol.*, vol. 41, no. 5, pp. 19–22, 2019.

[33] Z. Li et al., "Consideration by '75·8' extreme heavy rainfall event in Henan," *Meteorological Environ. Sci.*, vol. 38, no. 3, pp. 1–12, 2015.

[34] L. Lv, X. Wang, and H. Li, "Verification and analysis of SMS-WARMS forecast for'7·19' extraordinary rainstorm in Henan province," *Meteorological Environ. Sci.*, vol. 42, no. 1, pp. 101–109, 2019.

[35] X. Sha, M. Yang, J. Ding, Y. Xiao, and M. LI, "Rainstorm and hail weather of multi-region in Henan province on June 5, 2016," *Henan Sci.*, vol. 36, no. 5, pp. 765–770, 2018.

[36] H. Save, "CSR GRACE and GRACE-FO RL06 mascon solutions v02. 2020," Univ. Texas, Austin, TX, USA, vol. 10, 2020.

[37] J. Ran, P. Ditmar, L. Liu, Y. Xiao, R. Klees, and X. Tang, "Analysis and mitigation of biases in Greenland ice sheet mass balance trend estimates from GRACE mascon products," *J. Geophysical Res., Solid Earth*, vol. 126, no. 7, 2021, Art. no. e2020JB020880.

[38] T. Mayer-Gürr et al., "ITSG-grace2018: Monthly, daily and static gravity field solutions from GRACE," GFZ Data Services, 2018.

[39] S. Sun et al., "Applicability assessment of the 1998–2018 CLDAS multi-source precipitation fusion dataset over China," *J. Meteorological Res.*, vol. 34, no. 4, pp. 879–892, 2020.

[40] J. Li et al., "Impacts of land cover and soil texture uncertainty on land model simulations over the central Tibetan plateau," *J. Adv. Model. Earth Syst.*, vol. 10, no. 9, pp. 2121–2146, 2018.

[41] M. Grillakis, A. Koutroulis, J. Komma, I. Tsanis, W. Wagner, and G. Blöschl, "Initial soil moisture effects on flash flood generation–A comparison between basins of contrasting hydro-climatic conditions," *J. Hydrol.*, vol. 541, pp. 206–217, 2016.

[42] Y. Liu, W. Jing, S. Sun, and C. Wang, "Multi-scale and multi-depth validation of soil moisture from the China land data assimilation system," *IEEE J. Sel. Topics Appl. Earth Observ. Remote Sens.*, vol. 14, pp. 9913–9930, 2021.

[43] C. Shi, Z. Xie, H. Qian, M. Liang, and X. Yang, "China land soil moisture EnKF data assimilation based on satellite remote sensing data," *Sci. China Earth Sci.*, vol. 54, no. 9, pp. 1430–1440, 2011.

[44] Y. Shen and A. Xiong, "Validation and comparison of a new gauge-based precipitation analysis over mainland China," *Int. J. Climatol.*, vol. 36, no. 1, pp. 252–265, 2016.

[45] D. Long et al., "South-to-North water diversion stabilizing Beijing's groundwater levels," *Nature Commun.*, vol. 11, no. 1, pp. 1–10, 2020.

[46] Z. Gao, D. Long, G. Tang, C. Zeng, J. Huang, and Y. Hong, "Assessing the potential of satellite-based precipitation estimates for flood frequency analysis in ungauged or poorly gauged tributaries of China's Yangtze river basin," *J. Hydrol.*, vol. 550, pp. 478–496, 2017.

[47] V. Humphrey, L. Gudmundsson, and S. I. Seneviratne, "A global reconstruction of climate-driven subdecadal water storage variability," *Geophysical Res. Lett.*, vol. 44, no. 5, pp. 2300–2309, 2017.

[48] B. Li et al., "Global GRACE data assimilation for groundwater and drought monitoring: Advances and challenges," *Water Resour. Res.*, vol. 55, no. 9, pp. 7564–7586, 2019.

[49] J. Wu and X. Gao, "A gridded daily observation dataset over China region and comparison with the other datasets," *Chin. J. Geophys.*, vol. 56, no. 4, pp. 1102–1111, 2013.

[50] Y. Luo, C. Xu, Z. Chu, Q. Sun, and L. Chen, "Application of CN05.1 meteorological data in watershed hydrological simulation: A case study in the upper reaches of Kaidu river basin," *Adv. Climate Change Res.*, vol. 16, no. 3, pp. 287–295, 2020.

[51] L. Longuevergne, B. R. Scanlon, and C. R. Wilson, "GRACE hydrological estimates for small basins: Evaluating processing approaches on the high plains aquifer, USA," *Water Resour. Res.*, vol. 46, no. 11, 2010, Art. no. 2009WR008564.

[52] H. Kunstmann, C. Lorenz, B. Devaraju, M. J. Tourian, N. Sneeuw, and J. Riegger, "Large-scale runoff from landmasses: A global assessment of the closure of the hydrological and atmospheric water balances∗," *J. Hydrometeorology*, vol. 15, no. 6, pp. 2111–2139, 2014.

[53] R. P. Kornfeld et al., "GRACE-FO: The gravity recovery and climate experiment follow-on mission," *J. Spacecraft Rockets*, vol. 56, no. 3, pp. 931–951, 2019.
[54] R. E. Horton, "The role of infiltration in the hydrologic cycle," *Eos, Trans. Amer. Geophysical Union*, vol. 14, no. 1, pp. 446–460, 1933.
[55] H. Save, S. Bettadpur, and B. D. Tapley, "High-resolution CSR GRACE RL05 mascons," *J. Geophysical Res., Solid Earth*, vol. 121, no. 10, pp. 7547–7569, 2016.

Cuiyu Xiao received the bachelor's degree in surveying and mapping engineering from the East China University of Technology, Nanchang, China, in 2021. She is currently working toward the master's degree in surveying and mapping engineering with the China University of Geosciences, Wuhan, China.

Her research interests include combining near real-time precipitation data and GRACE observations to monitor flood events.

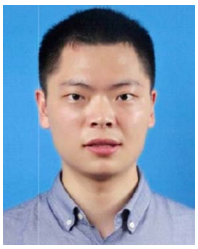

Yulong Zhong received the Ph.D. degree in geodesy and survey engineering from the Institute of Geodesy and Geophysics, Chinese Academy of Sciences, Wuhan, China, in 2018.

He is currently an Associate Professor with China University of Geosciences, Wuhan, China. His research interests focus on applying satellite gravimetry, including the groundwater storage change estimates, regional evapotranspiration estimate from GRACE, and separation of climate change and human activity in GRACE terrestrial water storage.

Wei Feng received the Ph.D. degrees in geodesy and geophysics from the Institute of Geodesy and Geophysics, Chinese Academy of Sciences, Wuhan, China, in 2013, and Toulouse III University, Toulouse, France, in 2015.

He is currently a Professor with the School of Geospatial Engineering and Science, Sun Yat-sen University, Zhuhai, China. His research interests include gravity inversion and interpretation based on ground and satellite gravimetry, especially the mass redistribution in the Earth system.

Wei Gao received the Ph.D. degree in cartography and geographical information engineering from China University of Geosciences, Wuhan, China, in 2010.

He is currently an Associate Professor with the School of Geography and Information Engineering, China University of Geosciences. His research interests include eco-environment and vegetation remote sensing and monitoring.

Zhonghua Wang received the master's degree in surveying and mapping engineering from Wuhan University, Wuhan, China, in 2015.

His research interests include analysis of engineering dewatering on the stability of foundation pits and analysis of the influence of engineering dewatering in structural monitoring for the operation of the rail transit project.

Min Zhong received the master's degree in solid earth geophysics from the Institute of Geodesy and Geophysics, Chinese Academy of Sciences, Wuhan, China, in 1990.

He is currently a Professor with the School of Geospatial Engineering and Science, Sun Yat-sen University, Zhuhai, China. His research interests include satellite gravity measurements, earth rotation measurements, satellite gravity data preprocessing, and climate change applications.

Bing Ji received the Ph.D. degree in satellite navigation from the Naval University of Engineering, Wuhan, China, in 2011.

He is currently an Associate Professor of Navigation with the Naval University of Engineering. His research interests include using gravity gradients for underwater navigation and exploration.